

**Showcasing research from the laboratory of Akos Vertes at the George Washington University.**

**Title: Polarization dependent fragmentation of ions produced by laser desorption from nanopost arrays**

Ion production from organic and biomolecules is essential for structure determination by mass spectrometry. Nanophotonic ion sources, such as nanopost arrays (NAPA), offer a new way of adjusting the internal energy of these ions based on the relative orientation between the posts and the plane of polarization of the desorption laser.

**As featured in:**



See Stolee and Vertes,  
*Phys. Chem. Chem. Phys.*, 2011, **13**, 9140.

Cite this: *Phys. Chem. Chem. Phys.*, 2011, **13**, 9140–9146

www.rsc.org/pccp

PAPER

## Polarization dependent fragmentation of ions produced by laser desorption from nanopost arrays

Jessica A. Stolee and Akos Vertes\*

Received 30th November 2010, Accepted 1st March 2011

DOI: 10.1039/c0cp02709j

Tailored silicon nanopost arrays (NAPA) enable controlled and resonant ion production in laser desorption ionization experiments and have been termed nanophotonic ion sources (Walker *et al.*, *J. Phys. Chem. C*, 2010, **114**, 4835–4840). As the post dimensions are comparable to or smaller than the laser wavelength, near-field effects and localized electromagnetic fields are present in their vicinity. In this contribution, we explore the desorption and ionization mechanism by studying how surface derivatization affects ion yields and fragmentation. We demonstrate that by increasing the laser fluence on derivatized NAPA with less polar surfaces that have decreased interaction energy between the structured silicon substrate and the adsorbate, the spectrum changes from exhibiting primarily molecular ions to showing a growing variety and abundance of fragments. The polarization angle of the laser beam had been shown to dramatically affect the ion yields of adsorbates. For the first time, we report that by rotating the plane of polarization of the desorption laser, the internal energy of the adsorbate can also be modulated resulting in polarization dependent fragmentation. This polarization effect also resulted in selective fragmentation of vitamin B<sub>12</sub>. To explore the internal energy of NAPA generated ions, the effect of the post aspect ratios on the laser desorption thresholds and on the internal energy of a preformed ion was studied. Elevated surface temperatures and enhanced near fields in the vicinity of high aspect ratio posts are thought to contribute to desorption and ionization from NAPA. Comparison of the fluence dependence of the internal energies of ions produced from nanoporous silicon and NAPA substrates indicates that surface restructuring or transient melting by the desorption laser is a prerequisite for the former but not for the latter.

### Introduction

Nanophotonics is a vigorously developing discipline because the nanostructures commensurate with the wavelength of the radiation confer unique capabilities for a wide range of applications such as telecommunications and biosensing.<sup>1,2</sup> A new approach is to make use of nanophotonic interactions to produce ions for mass spectrometric analysis.<sup>3,4</sup> When an electromagnetic field is coupled with nanostructures, strong light confinement and near-fields enhance the light–matter interactions<sup>5</sup> and can cause material desorption, ionization and ablation.<sup>6</sup> When biomolecules are adsorbed on nanostructures, such as laser-induced silicon micro-column arrays (LISMA)<sup>7</sup> or nanopost arrays (NAPA),<sup>8</sup> similar effects are thought to contribute to the desorption and ionization of these molecules. At this time, LISMA and NAPA are the only ion sources shown to exhibit nanophotonic ion production.

Matrix-assisted laser desorption ionization (MALDI) is an established ionization technique for the mass analysis of intact large biomolecules.<sup>9</sup> Due to the spectral interferences introduced by matrix-related ions in the low mass range, a multitude of matrix-free ionization platforms have emerged.<sup>10–14</sup> Desorption ionization on silicon (DIOS), which utilizes a nanoporous silicon substrate, has received the most attention due to its excellent sensitivity, simplicity, and high throughput.<sup>15</sup> The surface morphology of DIOS substrates, mainly the pore size and porosity, has been shown to play a large role in the efficiency of desorption and ionization of adsorbates.<sup>16,17</sup>

Nanophotonic ion production provides new opportunities compared to traditional ionization sources. For example, NAPA dimensions can be tailored to optimize ion production. Ion yield resonances were observed for nanoposts with specific high aspect ratios that exhibit strong local fields and elevated surface temperatures.<sup>8</sup>

Molecular ion yields from LISMA and NAPA also exhibit maxima as a function of polarization, analogous to the optical properties of nanoantennas.<sup>3,18–21</sup> This can be attributed to strong axial absorption of the electromagnetic field in the case

Department of Chemistry, The George Washington University, Washington, D.C. 20052, USA. E-mail: vertes@gwu.edu; Fax: +1 202-994-5873; Tel: +1 202-994-2717

of p-polarized beams, resulting in high ion yields, and insufficient excitation of the axial modes in the case of s-polarized radiation, producing little to no molecular ions. In contrast, polarization had no effect on the ion yields from MALDI.<sup>3</sup>

A third feature of nanophotonic ion sources is that the degree of fragmentation can be modulated by the laser fluence. At low laser intensities exclusively the molecular ion is observed, whereas at increased laser intensities structure specific fragmentation takes place.<sup>8,22</sup> Enhanced electromagnetic fields around the nanostructures, surface activation due to ion-surface collisions, and new reactive fragmentation channels are all thought to influence ionization and fragmentation from LISMA and NAPA. These mechanisms are fundamentally different from MALDI that produces low internal energy ions<sup>23,24</sup> and commonly relies on an additional activation step to induce fragmentation.<sup>25</sup> Similarly, DIOS produces molecular ions with some fragmentation and the ion internal energy is not affected by the desorption laser fluence.<sup>13,26</sup>

Control over molecular fragmentation is advantageous for elucidating the structure of biomolecules and for peptide sequencing. A crucial parameter governing the extent of fragmentation is the internal energy of the primary ions.<sup>27</sup> The ion internal energy can be gauged by applying the survival yield (SY) method to thermometer ions (TI).<sup>27,28</sup> These preformed ions allow the desorption step to be probed separately from the ionization step. The SY of the molecular ion is derived from the mass spectrum and corresponds to the ratio of the molecular ion intensity to the total ion intensity (the sum of the molecular and fragment ion intensities). This method has been used to investigate ion internal energies from a variety of ionization sources including electrospray ionization,<sup>29</sup> MALDI,<sup>23,24,30–33</sup> DIOS,<sup>17,26</sup> and LISMA.<sup>22</sup>

Fragmentation studies are not limited to thermometer ions, and the ion activation mechanisms and fragmentation of vitamin B<sub>12</sub> have also been studied by MALDI,<sup>34,35</sup> DIOS,<sup>36</sup> plasma desorption,<sup>37</sup> and laser desorption ionization.<sup>38</sup> In these experiments, vitamin B<sub>12</sub> acquires sufficient internal energy to readily fragment. Studying the propensity of vitamin B<sub>12</sub> fragmentation and comparing this with other methods can also give insight into the internal energy transfer from NAPA. A better understanding of the desorption and ionization mechanism from nanophotonic ion sources might enable us to adjust the transfer of laser energy for controlled ion yields and fragmentation.

In this contribution we use a threefold approach to study the desorption and fragmentation of adsorbates from NAPA. First, we investigate the use of derivatized NAPA for reduced fragmentation at low to moderate laser powers to gain an understanding of the influence of surface chemistry on ion disintegration. Second, we explore the effect of polarization on the ion yields and survival yields of thermometer ions. This gives insight into the polarization dependence of energy deposition and fragmentation on NAPA surfaces. The applicability of polarization dependent fragmentation to heterocyclic macrocycles is shown by studying the fragmentation pathways of vitamin B<sub>12</sub>. Thirdly, we systematically vary the NAPA post aspect ratios to study their effect on the laser threshold and fragmentation during the desorption process. Our results show that fragmentation can not only be adjusted

by varying the laser fluence and changing the NAPA post aspect ratios, but also by rotating the plane of polarization of the desorption laser.

## Experimental

### Materials

Aqueous stock solutions of Pro<sub>14</sub>-Arg (P14R) from Protea Biosciences, Inc. (Morgantown, WV) and vitamin B<sub>12</sub> (cyanocobalamin) purchased from Sigma Chemical Co. (St Louis, MO) were prepared in 50% methanol at 1 mg mL<sup>-1</sup> concentration and were diluted as necessary. The chloride salt of the 4-methyl-benzylpyridinium (4M) thermometer ion (TI) was custom synthesized by Celestial Specialty Chemicals (Nepean, Ontario, Canada). Stock solutions were prepared in 50% methanol and diluted to 0.7 μM. All solutions were made using deionized water (18.2 M Ω cm) produced with an E-pure system (Barnstead, Dubuque, IA) and reagent grade methanol purchased from Sigma Chemical Co. (St Louis, MO). For the derivatization of the NAPA, (perfluorophenyl)-propyldimethylchlorosilane was purchased from Gelest, Inc. (Morrisville, PA).

### Nanofabrication of NAPA

A detailed description of NAPA fabrication can be found elsewhere.<sup>8</sup> Briefly, silicon wafers with a range of resistivities (0.005–100 Ω cm) were spin-coated with Zep520A resist. Patterns designating the top view of NAPA, with diameters, *D*, between 100 nm and 250 nm and periodicities, *P*, of 337 nm and 674 nm, were rendered on the wafers by e-beam lithography (JBX-9300, JEOL, Peabody, MA). The exposed resist was then removed and the wafers were coated with 10 nm of chromium using vacuum deposition. Following the removal of the unexposed resist that was coated with chromium, posts of ~1000 nm heights were produced with an Oxford PlasmaLab100 RIE reactive ion etching system. For surface characterization of the structures a dual beam scanning electron microscope (SEM) (Nova Nanolab 600, FEI, Hillsboro, OR) was used.

Optionally, perfluorophenyl (PFP)-derivatized NAPA were produced by oxidizing the surfaces by exposure to ozone, covering the oxidized NAPA with ~15 μL of (perfluorophenyl)-propyldimethylchlorosilane, and baking the surfaces in an oven for 30 min. The derivatized NAPA were thoroughly rinsed with methanol and deionized water and air-dried.

### Mass spectrometry

A 0.5 μL drop of the sample solution was deposited on the NAPA surface and air-dried prior to mass spectrometry experiments. Laser desorption and ionization was performed using a high-resolution curved field reflectron time-of-flight mass spectrometer (Axima CFR, Shimadzu-Kratos, Manchester, UK). Averaged spectra were acquired from 100 laser shots in reflectron mode using delayed ion extraction with 2.5 kV extraction voltage, 20 kV accelerating voltage, and a 100 ns delay.

Experiments using plane polarized laser beams were conducted using a home-built linear time-of-flight mass spectrometer.

Radiation from a 4 ns pulse length nitrogen laser ( $\lambda = 337$  nm) (VSL-337ND, Laser Science Inc., Newton, MA) was polarized by a Glan–Taylor calcite polarizer. A variable neutral density filter was used to maintain a constant pulse energy while the plane of polarization was rotated. The areas of sample specific peaks were integrated from averaged spectra to obtain the ion yields.

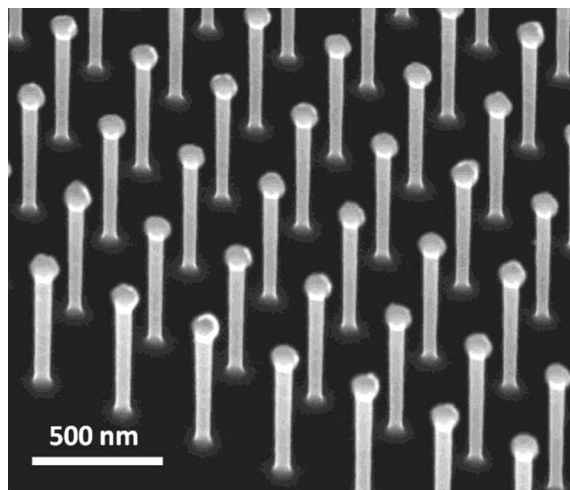
## Results and discussion

Fig. 1 shows a representative SEM image of a NAPA segment with post diameter,  $D$ , periodicity,  $P$ , and height,  $H$ , of 100 nm, 337 nm, and 1000 nm respectively. The dimensions of NAPA are precisely controlled in the nanofabrication process and the resulting high aspect ratio structures have vertical walls with no noticeable taper. SEM images also verified that the NAPA remained intact after laser desorption experiments, although for posts with diameters smaller than the thermal diffusion length transient melting is still possible.<sup>39</sup>

### Fragmentation from surface derivatized NAPA

It has been shown that both low- and high-energy fragmentation channels are active in NAPA.<sup>8</sup> To further explore this finding, we introduce chemical derivatization to change the interaction energy between the adsorbate and the surface. Silylation is a reliable method for the chemical modification of silicon surfaces and the diversity of available reagents provides a means to control the polarity of the substrate. Perfluorophenyl (PFP)-derivatization creates less polar and more hydrophobic surfaces and results in decreased interaction energy between the structured silicon substrate and the adsorbate. As a consequence, for other silicon-based platforms lower laser desorption thresholds have been observed.<sup>15,22</sup>

Similarly, NAPA derivatized with PFP results in up to ten times higher peptide molecular ion yields than native NAPA (data not shown). Although the mechanism is unclear, native NAPA is also capable of producing structure specific peptide fragmentation. To characterize fragmentation from derivatized



**Fig. 1** After reactive ion etching, SEM imaging confirms the uniform distribution and negligible tapering of high aspect ratio posts in a NAPA with  $D = 100$  nm,  $P = 337$  nm, and  $H = 1000$  nm.

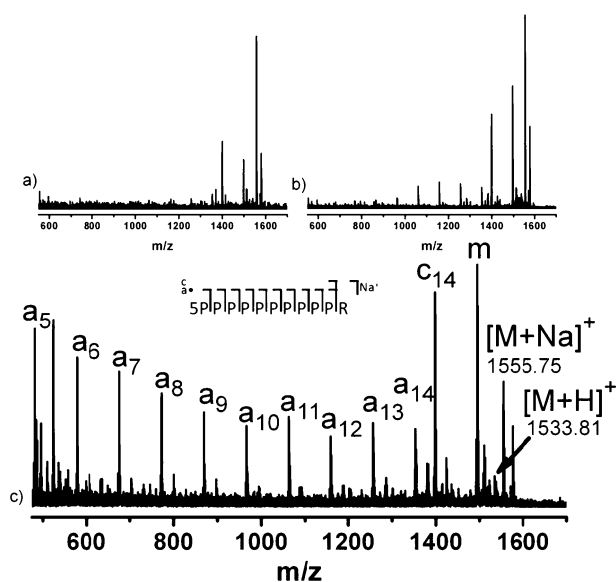


**Fig. 2** (a) Mass spectrum of P14R from PFP-NAPA at a laser power of 75 (arbitrary units) shows minimal fragmentation. (b) As the power is increased to 80 fragments begin to emerge. (c) At a laser power of 130, structure specific fragmentation, corresponding to the sodiated N-terminal fragment ions (a- and c-type), is observed.

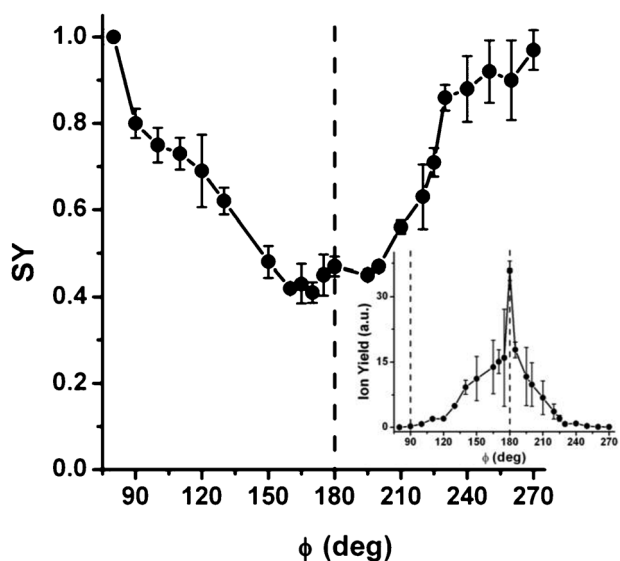
NAPA, the labile synthetic peptide Pro<sub>14</sub>-Arg (P14R  $m/z$  of 1533.86) was used. P14R has a basic arginine at the C-terminus and in MALDI experiments it is known to undergo post-source fragmentation at the proline residues.<sup>40</sup> The nomenclature of peptide fragmentation is described in ref. 41.

Fig. 2a shows the mass spectrum of P14R from PFP-NAPA at relatively low laser power (75 in arbitrary units). The most abundant peak is the sodiated P14R molecule. Additionally, C<sub>14</sub> ions are present due to the loss of the arginine residue. This indicates that the low-energy fragmentation channels may already be activated at this power. As the laser power is increased to 80, high mass P14R fragments begin to appear (Fig. 2b). A significantly increased overall abundance of fragment ions can be observed if the laser power is further increased to a high value of 130 (Fig. 2c), whereas the molecular and quasimolecular ions decrease in intensity. These fragments correspond to sodiated a-type ions, a result of proline residue cleavage from the N-terminus, and b-type ions that appear with lower intensity (not labeled).

This latter fragmentation pattern dramatically differs from that of MALDI, in which the intensity of the y-type ions precipitously diminishes as subsequent prolines are lost. In the case of PFP-NAPA, the fragment ion intensities increase with sequential proline losses. This suggests that at this laser power, high-energy fragmentation channels are activated.

### Polarization dependent fragmentation

The polarization of the desorption laser has a profound effect on the ionization processes in nanophotonic ion sources. For peptides and small organic molecules, p-polarized radiation generates high molecular ion yields, whereas s-polarized laser pulses result in little or no ion production.<sup>3,8</sup> To investigate the effect of polarization on the internal energy transfer on NAPA during the desorption step, the survival yield method was



**Fig. 3** As the polarization angle,  $\phi$ , of the desorption laser is rotated from s-polarized (at  $90^\circ$ ) to p-polarized ( $180^\circ$ ) the degree of fragmentation of the 4M TI, represented by the survival yield, reaches a minimum. The inset shows that the ion yield of the 4M TI rises sharply for p-polarized radiation.

applied using the 4M thermometer ion. As 4M is a preformed ion, it enables us to separate the desorption and the ionization steps and focus only on the former. The mass spectra of 4M exhibit a single fragmentation channel and the only peaks that are present are the molecular ion and a fragment ion, which is the result of a pyridine loss.

First, the total ion yield of the 4M thermometer ion was measured as the polarization angle,  $\phi$ , was rotated from s- to p-polarized. The inset in Fig. 3 shows that the total ion yield of 4M exhibits a maximum for the p-polarized ray and the ion yield decreases significantly as the beam is rotated to s-polarized. At  $180^\circ$  there is a sharp maximum with an order of magnitude increase compared to the s-polarized signal. This implies that the angle of polarization affects the ability of NAPA to absorb the laser energy resulting in efficient desorption of the adsorbate.

In the laser desorption process, the energy transfer from NAPA to the adsorbate can be assessed by monitoring the SY as a function of the angle of polarization. Fig. 3 shows a pronounced minimum in the SY when the desorption laser is p-polarized. As the plane of polarization is rotated from s- to p-polarized, the SY starts from 1, indicating no fragmentation, and decreases to 0.4, indicating significant fragmentation. This drastic fall in the SY indicates a significant rise in the internal energy that is a strong function of the polarization. As a consequence, the polarization can be adjusted to vary the degree of fragmentation while still maintaining sufficient ion yields.

The polarization dependence of ion yields from NAPA reveals that the axial currents induced in the posts play a large role in the desorption process. As the 337 nm radiation corresponds to 889 THz, the DC conductivity of the silicon wafers should be irrelevant in the energy deposition. Indeed, desorption experiments on NAPA with a range of DC resistivities

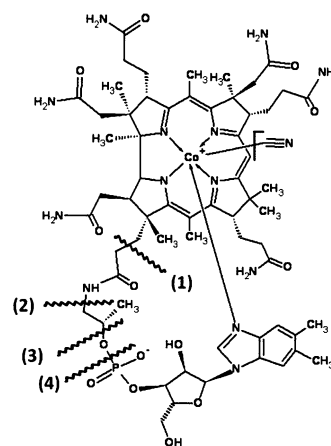


**Fig. 4** Vitamin B<sub>12</sub> molecular structure showing the losses associated with four of the fragment ions detected in NAPA experiments. Fragment ion (1) corresponds to  $[(M + K)\text{-CN-DMBI-pentose-PO}_4\text{-CH}_2\text{CONHCH}_2\text{CHCH}_3]^+$  at  $m/z$  913, (2) is  $[\text{M-CN-DMBI-pentose-PO}_4\text{-C}_3\text{H}_6]^+$  at  $m/z$  931, (3) is  $[\text{M-CN-DMBI-pentose-PO}_4]^+$  at  $m/z$  972 and (4) is  $[\text{M-CN-DMBI-pentose-PO}_3]^+$  at  $m/z$  989, where DMBI is dimethylbenzimidazole.

between  $0.005 \Omega \text{ cm}$  and  $100 \Omega \text{ cm}$  revealed minimal change in the SYs (results not shown).

To test the application of adjusting fragmentation *via* polarization, a neutral molecule, vitamin B<sub>12</sub> (see Fig. 4), was chosen as a model compound. Vitamin B<sub>12</sub> was selected because it fragments readily in laser desorption experiments and comparisons can be made with other methods that have studied its fragmentation. Direct laser desorption ionization of vitamin B<sub>12</sub> from polished silicon produced no molecular ions from the adsorbate. With PFP-NAPA, positive mode mass spectrometric experiments at high laser power resulted in 9 fragments along with the molecular ion. These previously observed species include two of the three fragment ions detected with DIOS, four of the five ions observed with traditional MALDI, and eight of the thirteen ions produced in a postionization experiment.<sup>36,42</sup> At lower laser fluences the four most abundant peaks observed are at  $m/z$  913,  $m/z$  931,  $m/z$  972, and  $m/z$  989 that correspond to fragments (1), (2), (3) and (4), respectively, in Fig. 4. The molecular structure of vitamin B<sub>12</sub> along with these four losses is shown in Fig. 4 and a mass spectrum of these peaks is shown in the inset of Fig. 5.

The ion yields of two fragment peaks from PFP-NAPA were studied as a function of the polarization angle (see Fig. 5). While most of the fragment intensities only exhibit a weak maximum for the p-polarized beam, the peak at  $m/z$  972 shows a strong resonance. This fragment is formed by the loss of the 5,6-dimethylbenzimidazolyl nucleotide, which is the main fragmentation channel in these experiments indicating that the corresponding C–O bond is the weakest in the structure. Therefore it exhibits the strongest fragmentation response to increasing the internal energy of the molecule. This species is also a characteristic vitamin B<sub>12</sub> fragment in DIOS experiments, and its formation has been explained by the absorption maximum of the molecule at 361 nm and the dissociation of the photoactivated molecule.<sup>36</sup> In the case of NAPA, however, the fragmentation likely follows different

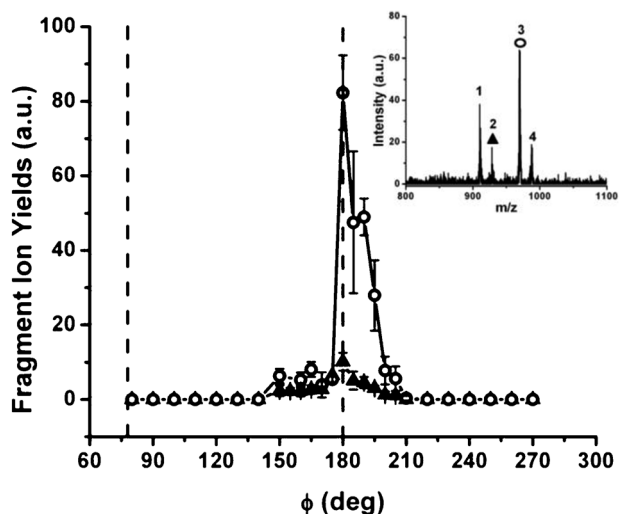


**Fig. 5** Ion yields for two of the most prominent vitamin B<sub>12</sub> fragments from PFP-NAPA as a function of polarization angle,  $\phi$ , at a constant fluence. The mass spectrum in the inset shows the peaks of four vitamin B<sub>12</sub> fragments and the ion yields of the two peaks with symbols are shown. The numbers above the peaks correspond to the losses shown in Fig. 4.

pathways. As we have shown in the case of 4M TI, the enhanced energy deposition into the posts for p-polarized beams results in higher internal energy. This mechanism is also expected to be active for the vitamin B<sub>12</sub> molecule. In addition, the field enhancement around the posts is also accentuated for the p-polarized case, potentially resulting in stronger field ionization.<sup>43</sup> Thus, in addition to changing the laser power, the polarization of the laser can also be utilized for the adjustable fragmentation of a molecule.

Other mechanisms of vitamin B<sub>12</sub> ion excitation have been proposed. In UV-MALDI, the internal energy transfer was found to primarily depend on the matrix used, and photodissociation was found not to play a role in the fragmentation.<sup>34</sup> Likewise, photodissociation does not explain the polarization dependent fragmentation from NAPA. Instead, the interaction of the electromagnetic field with the posts clearly plays a large role in the ionization and fragmentation of the molecules desorbed from NAPA.

Optical antennas show strong resonances when the electromagnetic field is polarized along the axis of the antenna structures whereas no such resonances are observed when the light is perpendicular to the antenna's long axis.<sup>20,44</sup> In NAPA, the polarization dependence has been explained in terms of strong axial absorption of p-polarized laser radiation. Results from both the thermometer ion and vitamin B<sub>12</sub> studies show that the internal energy of the adsorbate is preferentially increased for p-polarized radiation, as shown by the increased fragmentation. The fragmentation and ion yield resonances from NAPA can both be explained by the energy deposition into the posts and the electric field intensity enhancements around them. The polarization dependence of fragmentation shows the importance of the electric field enhancements on fragmentation, insight that cannot be derived from the fluence dependence of fragmentation alone.

### Post aspect ratio and surface polarity effects

To further our understanding of the desorption mechanism, SYs from native and derivatized NAPA with post aspect ratios ( $H/D$ ) ranging from 10 and 4 with periodicities of 337 nm and 674 nm were investigated. The points with the lowest fluence for the SY curves in Fig. 6 also represent the desorption threshold for the corresponding post geometry. For both native and PFP-derivatized NAPA, the minimum laser fluence required to desorb the 4M TI shifts to higher values as the post diameter increases, *i.e.*, as  $H/D$  decreases (see Fig. 6). For example, in the case of the thinnest posts with diameters of 100 nm ( $H/D = 10$ ), 4M is desorbed with a fluence of less than 5 mJ cm<sup>-2</sup>, whereas almost 60 mJ cm<sup>-2</sup> is required to desorb 4M from 250 nm posts ( $H/D = 4$ ).

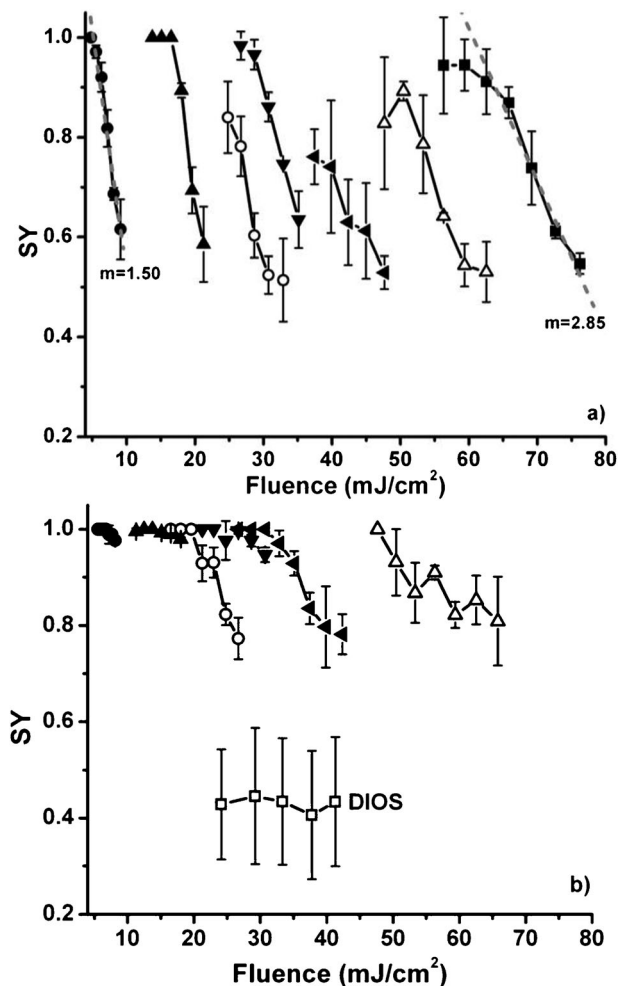


**Fig. 6** Survival yields of 0.35 pmol of 4M TI from (a) native NAPA and (b) PFP-derivatized NAPA with  $P = 337$  nm for  $H/D = 10$  (●), 8 (▲), and 6.7 (▼), and  $P = 674$  nm for  $H/D = 5.7$  (○), 5 (◄), 4.4 (△) and 4 (■), and a resistivity of 10–100 Ω cm. In panel (a) the SYs from native NAPA show a steep decline, from values close to 1 to between 0.5 and 0.6, as the laser fluence is increased. In (b) the SYs from PFP-NAPA with  $P = 337$  nm remain close to 1 whereas SYs from NAPA with  $P = 674$  nm decrease from 1 to 0.8. In contrast, the SY of 35 pmol of 4M TI desorbed from PFP-derivatized DIOS substrates is significantly lower, SY = ~0.4, and it shows no change with increasing fluence (data from ref. 26).

This 12-fold change in the desorption threshold fluence can be attributed to enhanced near fields in the vicinity of the high aspect ratio posts and to the higher surface temperatures observed for posts with diameters below the thermal diffusion length.<sup>8,45</sup>

For the range of post diameters studied, SYs from native NAPA decrease as the laser fluence is increased, Fig. 6a. This decline correlates to higher internal energy transfer due to elevated post surface temperatures at higher laser fluences. In addition, when the post diameters are smaller than the thermal diffusion length, dissipation of the deposited laser energy in the posts is obstructed by radial confinement. From Fig. 6a it can be observed that the SY drops at a faster rate as the post diameters are decreased (see the slopes of the fitted lines in Fig. 6a). The thinner posts have lower conductive thermal loss, reach higher maximum surface temperatures and heat more uniformly than the thicker ones. These high surface temperatures provide a stronger driving force for the energy transfer to the adsorbate.

The effect of surface derivatization on the internal energy of the 4M TI is shown in Fig. 6b. It is evident that PFP-derivatization of NAPA reduces the internal energy transfer to the adsorbate, as indicated by the generally higher SYs. The SY values either remain close to one for thinner posts or decrease only moderately to around 0.8 for the thicker ones. In addition, the threshold laser fluence shifts to slightly lower values for derivatized NAPA. These effects are due to the reduced interaction energy between the polar TI and the derivatized NAPA surface that is apolar.

The SY values and their fluence dependence for 4M desorbed from PFP-NAPA are in stark contrast to observations on PFP-DIOS, for which a constant SY of around 0.4 has been observed independent of the laser fluence.<sup>26</sup> In DIOS experiments the lack of fluence dependence on the internal energy of the ions was attributed to the limited interaction time between the DIOS surface and the adsorbates due to rapid heating. Energy deposition in NAPA will also cause the post temperatures to increase rapidly resulting in the fast desorption of the TI. Therefore, this does not explain the differences in the magnitude and fluence dependence of the SYs between the two methods. This drastic disparity might be attributed to differences in the morphology of the DIOS and NAPA structures. While DIOS exhibits 20 to 100 nm pores<sup>46</sup> separated by pore walls of similar thickness, the studied NAPA structures have 100 to 250 nm posts separated by approximately twice as wide troughs. The thin pore walls of the DIOS structure reach temperatures above the melting point in the fluence range of interest.<sup>46,47</sup> These high temperatures result in the reduced SYs observed for DIOS. For the significantly thicker posts of NAPA, however, the surface temperatures remain lower at similar fluences explaining the higher SYs.

These observations and Fig. 6b point to the fundamental difference between the ion production from DIOS and NAPA substrates. Whereas for DIOS surface restructuring or transient melting by the desorption laser seems to be a prerequisite for ion production, for NAPA there is no such requirement. These differences are reflected in the absolute values and the fluence dependence of the SYs.

## Conclusions

Nanophotonic ion sources such as LISMA and NAPA offer new means of coupling laser radiation to nanostructures for ion production. The interaction between the electromagnetic radiation and the nanoposts can be manipulated to induce desorption, ionization, and fragmentation. We demonstrate that NAPA enables adjustable structure specific fragmentation as a function of the laser fluence. This allows enhanced structure identification in the mass spectrometry of organic molecules and for peptide sequencing without using an additional ion activation step to induce fragmentation.

We have found that the desorption yield of preformed ions and neutral molecules strongly depends on the polarization of the laser beam and for the first time we have also demonstrated that the internal energy transfer, and consequently the degree of fragmentation, are also affected by polarization. It was shown that certain fragment ions are more sensitive to polarization, and this may lead to a method that can preferentially fragment a molecule. This enhanced control over fragmentation opens new possibilities in structure elucidation of organic compounds using mass spectrometry. In particular the ability to adjust fragmentation *via* the polarization angle might obviate the need for collisional activation in tandem mass spectrometry. Conversely, simple single stage mass spectrometers can be used to explore the structure of simple organic compounds.

Investigating the impact of the NAPA dimensions on the internal energy of adsorbates gave insight into the mechanism of desorption from NAPA. Thermal confinement in thin posts leads to more efficient desorption and fragmentation. Findings show that the internal energy of the adsorbate increases as the fluence is raised. This is consistent with biomolecule fragmentation at high laser fluences. High surface temperatures and enhanced near fields around the posts can contribute to the desorption and ionization. By modifying the surface polarity, the interaction energy between the adsorbate and NAPA is affected, and less internal energy is transferred to the thermometer ions.

Comparison of the ion yields and SYs from NAPA and DIOS substrates reveals fundamental differences. Whereas restructuring and transient melting are a prerequisite for ion production from DIOS, they do not seem to play a role in the case of NAPA.

We have demonstrated that nanophotonic interactions offer new means for the production of ions from organic molecules and biopolymers with enhanced control over their internal energy. The NAPA substrates in this study are an example of such nanophotonic ion sources. Better understanding of desorption and ionization from these ion sources will enable even greater control of the ion yields.

## Acknowledgements

The authors are grateful for the financial support from the Chemical Sciences, Geosciences and Biosciences Division within the Office of Basic Energy Sciences of the U.S. Department of Energy (DE-FG02-01ER15129) and from Protea Biosciences, Inc. Support from the Department of Energy does

not constitute an endorsement of the views expressed in the article. J. A. S. is thankful for the scholarship award from the Achievement Rewards for College Scientists Foundation, Inc. (ARCS). NAPA were nanofabricated at Oak Ridge National Laboratory's Center for Nanophase Materials Sciences under a User Agreement (CNMS2008-249) and the authors appreciate the help of Scott T. Retterer and Bennett N. Walker.

## Notes and references

- 1 E. Ozbay, *Science*, 2006, **311**, 189–193.
- 2 S. Lal, S. Link and N. J. Halas, *Nat. Photonics*, 2007, **1**, 641–648.
- 3 B. N. Walker, T. Razunguzwa, M. Powell, R. Knochenmuss and A. Vertes, *Angew. Chem., Int. Ed.*, 2009, **48**, 1669–1672.
- 4 R. Stockle, P. Setz, V. Deckert, T. Lippert, A. Wokaun and R. Zenobi, *Anal. Chem.*, 2001, **73**, 1399–1402.
- 5 H. F. Hamann, A. Gallagher and D. J. Nesbitt, *Appl. Phys. Lett.*, 2000, **76**, 1953–1955.
- 6 A. Plech, V. Kotaidis, M. Lorenc and J. Boneberg, *Nat. Phys.*, 2006, **2**, 44–47.
- 7 Y. Chen and A. Vertes, *Anal. Chem.*, 2006, **78**, 5835–5844.
- 8 B. N. Walker, J. A. Stolee, D. L. Pickel, S. T. Retterer and A. Vertes, *J. Phys. Chem. C*, 2010, **114**, 4835–4840.
- 9 M. Karas and F. Hillenkamp, *Anal. Chem.*, 1988, **60**, 2299–2301.
- 10 T. R. Northen, O. Yanes, M. T. Northen, D. Marrinucci, W. Uritboonthai, J. Apon, S. L. Golledge, A. Nordstrom and G. Siuzdak, *Nature*, 2007, **449**, 1033–U1033.
- 11 E. P. Go, J. V. Apon, G. H. Luo, A. Saghatelian, R. H. Daniels, V. Sahi, R. Dubrow, B. F. Cravatt, A. Vertes and G. Siuzdak, *Anal. Chem.*, 2005, **77**, 1641–1646.
- 12 J. D. Cui, D. J. Hayes, S. J. Fonash, K. N. Brown and A. D. Jones, *Anal. Chem.*, 2001, **73**, 1292–1295.
- 13 J. Wei, J. M. Buriak and G. Siuzdak, *Nature*, 1999, **399**, 243–246.
- 14 L. Sainiemi, H. Keskinen, M. Aromaa, L. Luosujarvi, K. Grigoras, T. Kotiaho, J. M. Makela and S. Franssila, *Nanotechnology*, 2007, **18**, 7.
- 15 S. A. Trauger, E. P. Go, Z. X. Shen, J. V. Apon, B. J. Compton, E. S. P. Bouvier, M. G. Finn and G. Siuzdak, *Anal. Chem.*, 2004, **76**, 4484–4489.
- 16 R. A. Kruse, X. L. Li, P. W. Bohn and J. V. Sweedler, *Anal. Chem.*, 2001, **73**, 3639–3645.
- 17 Y. S. Xiao, S. T. Retterer, D. K. Thomas, J. Y. Tao and L. He, *J. Phys. Chem. C*, 2009, **113**, 3076–3083.
- 18 P. Muhlschlegel, H. J. Eisler, O. J. F. Martin, B. Hecht and D. W. Pohl, *Science*, 2005, **308**, 1607–1609.
- 19 K. B. Crozier, A. Sundaramurthy, G. S. Kino and C. F. Quate, *J. Appl. Phys.*, 2003, **94**, 4632–4642.
- 20 H. Fischer and O. J. F. Martin, *J. Eur. Opt. Soc., Rapid Publ.*, 2008, **3**, 4.
- 21 A. G. Curto, G. Volpe, T. H. Taminiu, M. P. Kreuzer, R. Quidant and N. F. van Hulst, *Science*, 2010, **329**, 930–933.
- 22 J. A. Stolee, Y. Chen and A. Vertes, *J. Phys. Chem. C*, 2010, **114**, 5574–5581.
- 23 G. H. Luo, I. Marginean and A. Vertes, *Anal. Chem.*, 2002, **74**, 6185–6190.
- 24 V. Gabelica, E. Schulz and M. Karas, *J. Mass Spectrom.*, 2004, **39**, 579–593.
- 25 K. F. Medzihradsky, J. M. Campbell, M. A. Baldwin, A. M. Falick, P. Juhasz, M. L. Vestal and A. L. Burlingame, *Anal. Chem.*, 2000, **72**, 552–558.
- 26 G. H. Luo, Y. Chen, G. Siuzdak and A. Vertes, *J. Phys. Chem. B*, 2005, **109**, 24450–24456.
- 27 K. Vekey, *J. Mass Spectrom.*, 1996, **31**, 445–463.
- 28 F. Derwa, E. Depauw and P. Natalis, *Org. Mass Spectrom.*, 1991, **26**, 117–118.
- 29 C. Collette, L. Drahos, E. De Pauw and K. Vekey, *Rapid Commun. Mass Spectrom.*, 1998, **12**, 1673–1678.
- 30 J. F. Greisch, V. Gabelica, F. Remacle and E. De Pauw, *Rapid Commun. Mass Spectrom.*, 2003, **17**, 1847–1854.
- 31 A. Vertes, G. H. Luo, L. Ye, Y. Chen and I. Marginean, *Appl. Phys. A: Mater. Sci. Process.*, 2004, **79**, 823–825.
- 32 G. Luo, I. Marginean, L. Ye and A. Vertes, *J. Phys. Chem. B*, 2008, **112**, 6952–6956.
- 33 E. Stevenson, K. Breuker and R. Zenobi, *J. Mass Spectrom.*, 2000, **35**, 1035–1041.
- 34 G. R. Kinsel, L. M. Preston and D. H. Russell, *Biol. Mass Spectrom.*, 1994, **23**, 205–211.
- 35 L. He, G. Wei and K. K. Murray, *J. Am. Soc. Mass Spectrom.*, 1997, **8**, 140–147.
- 36 I. Shmygol', S. Snegir and V. Pokrovskii, *Theor. Exp. Chem.*, 2007, **43**, 272–277.
- 37 J. F. Blankenship, M. J. VanStipdonk and E. A. Schweikert, *Rapid Commun. Mass Spectrom.*, 1997, **11**, 143–147.
- 38 D. J. Rousell, S. M. Dutta, M. W. Little and K. K. Murray, *J. Mass Spectrom.*, 2004, **39**, 1182–1189.
- 39 B. N. Walker, J. A. Stolee, D. L. Pickel, S. T. Retterer and A. Vertes, *Appl. Phys. A: Mater. Sci. Process.*, 2010, **101**, 539–544.
- 40 B. Paizs and S. Suhai, *Mass Spectrom. Rev.*, 2005, **24**, 508–548.
- 41 K. Biemann, *Biomed. Environ. Mass Spectrom.*, 1988, **16**, 99–111.
- 42 T. Solouki and D. H. Russell, *Appl. Spectrosc.*, 1993, **47**, 211–217.
- 43 J. F. Wang, M. S. Gudiksen, X. F. Duan, Y. Cui and C. M. Lieber, *Science*, 2001, **293**, 1455–1457.
- 44 E. Cubukcu, E. A. Kort, K. B. Crozier and F. Capasso, *Appl. Phys. Lett.*, 2006, **89**, 3.
- 45 J. A. Stolee, B. N. Walker, Y. Chen and A. Vertes, *AIP Conf. Proc.*, 2010, **1278**, 98–110.
- 46 T. R. Northen, H. K. Woo, M. T. Northen, A. Nordstrom, W. Uritboonthai, K. L. Turner and G. Siuzdak, *J. Am. Soc. Mass Spectrom.*, 2007, **18**, 1945–1949.
- 47 V. Y. Timoshenko, T. Dittrich, I. Sieber, J. Rappich, B. V. Kamenev and P. K. Kashkarov, *Phys. Status Solidi A*, 2000, **182**, 325–330.